LRP 510/95 January 1995

DIRECT MEASUREMENT OF THE DAMPING OF TOROIDICITY INDUCED ALFVEN EIGENMODES

A. Fasoli, J.B. Lister, J.-M. Moret, S. Sharapov,
D. Borba, G. Bosia, D.J. Campbell, J.A. Dobbing,
C. Gormezano, J. Jacquinot, P. Lavanchy,
Ph. Marmillod and A. Santagiustina

submitted to
Physical Review Letters

Direct Measurement of the Damping of Toroidicity Induced Alfvén Eigenmodes

A.Fasoli[1], J.B.Lister[1], J.-M.Moret[1], S.Sharapov, D.Borba, G.Bosia, D.J.Campbell, J.A.Dobbing, C.Gormezano, J.Jacquinot, P. Lavanchy[1], P.Marmillod[1] and A.Santagiustina

JET Joint Undertaking, Abingdon, Oxon OX14 3EA, UK.

[1]*Centre de Recherches en Physique des Plasmas, Association EURATOM-Confederation Suisse, Ecole Polytechnique Federale de Lausanne, 1015 Lausanne, Switzerland.*

Abstract

This Letter presents the first direct experimental measurements of the damping of Toroidicity induced Alfvén Eigenmodes (TAE), carried out in the JET tokamak. These measurements were obtained during the first experiments to drive these modes with antennas external to a tokamak plasma. Different regimes corresponding to different dominant TAE absorption mechanisms with a wide range of damping rates, $10^{-3} \lesssim \gamma/\omega \lesssim 10^{-1}$, have been identified in ohmically heated plasma discharges using this new active diagnostic for Alfvén eigenmodes.

Direct Measurement of the Damping of Toroidicity Induced Alfvén Eigenmodes

A.Fasoli[1], J.B.Lister[1], J.-M.Moret[1], S.Sharapov, D.Borba, G.Bosia, D.J.Campbell, J.A.Dobbing, C.Gormezano, J.Jacquinot, P. Lavanchy[1], P.Marmillod[1] and A.Santagiustina

JET Joint Undertaking, Abingdon, Oxon OX14 3EA, UK.

[1]*Centre de Recherches en Physique des Plasmas, Association EURATOM-Confederation Suisse, Ecole Polytechnique Federale de Lausanne, 1015 Lausanne, Switzerland.*

In ignited magnetically confined plasmas, the large amount of energy and the steep pressure gradients associated with alpha particles created by fusion reactions can lead to the excitation, via wave-particle interactions, of global electromagnetic modes which may be deleterious for plasma performance. In tokamaks, Alfvén eigenmodes exist as discrete modes in the gaps of the shear Alfvén wave continua, induced by toroidal geometry (TAE) [1], elliptical cross section (EAE) [2] and finite beta effects (BAE) [3,4]. These modes are of particular concern as they can be driven through inverse Landau damping by resonant fast particles, having velocities $v \sim v_{Alfvén}$, where $v_{Alfvén}=B_{tor}/(\mu_0\rho)^{1/2}$, ρ being the mass density and B_{tor} the toroidal magnetic field [5]. The alpha particles created by fusion reactions will satisfy this resonance condition during their slowing-down, but resonant particles will also be created by Neutral Beam Injection Heating or Ion Cyclotron Resonance Heating. If the linear damping rate of an

eigenmode is smaller than the growth rate due to driving by these fast particles, the mode becomes unstable and reaches an amplitude limited only by non-linear damping or modifications of the velocity distributions or the equilibrium profiles. The oscillating electromagnetic field associated with these eigenmodes can then affect the orbits of the resonant fast particles themselves, creating anomalous transport. Such transport may lead to an increase of the reactivity required for ignition, as well as to localised energy deposition and significant first wall damage [6].

In order to assess the linear stability of Alfvén eigenmodes, both driving and damping effects must be investigated. The theoretical evaluation of these terms is made extremely intricate by the concurrence of MHD and kinetic effects. The predictions of the damping rates vary by more than one order of magnitude, according to the *a priori* assumptions characterising different models. A direct measurement of the Alfvén eigenmode damping rate and investigations into the relevant absorption mechanisms, such as reported in this Letter, therefore assume a fundamental importance.

Existing experimental results on the role of Alfvén eigenmodes in affecting transport in tokamak plasmas also vary considerably. TAE, EAE and BAE activity, driven by energetic particles, has been reported for NBI and ICRH heated discharges in different tokamak experiments [4,7-10]. Fast particle losses together with a sudden reduction of the neutron production rate have been observed at the same time as bursts of MHD activity which were tentatively attributed to Alfvén eigenmodes [6]. In similar experiments in deuterium-tritium plasmas, no increase in the lost alpha flux was observed in the presence of TAE activity [11]. Such passive studies, although providing frequency and mode spectra as well as some information on the instability thresholds and

saturation levels, can not provide quantitative estimates of the damping and driving of the Alfvén eigenmodes.

A more complete picture of the MHD activity in this Alfvén range of frequencies can be obtained from measurements of the plasma response to external perturbations. Combining excitation by external antennas with coherent detection of various probing signals at the plasma edge and in the core has created the active diagnostic for Alfvén eigenmodes on the JET tokamak [12] which has the unique advantage of providing a direct measurement of the damping rates of the Alfvén eigenmodes in various plasma conditions. This method constitutes a tool for an identification of the different damping mechanisms which will determine the instability threshold of the Alfvén eigenmodes in reactor relevant plasma conditions. Similar experiments had previously only been carried out in the discrete Alfvén wave range of frequencies on the TCA, PETULA and TEXTOR tokamaks [13-15]. In this Letter we present the experimental arrangement and method, results on the identification of the eigenmode dispersion relation and the first measurements of the damping rate for Toroidicity induced Alfvén Eigenmodes.

The JET saddle coils, 4 above and 4 below the plasma, situated 90^0 apart toroidally and covering poloidal and toroidal extensions of about 60^0 and 90^0 [16], are used as external antennas to excite the Alfvén eigenmodes. The Alfvén eigenmode exciter and detection systems have been developed to cover the frequency range from 20 to 500 kHz, including BAE, TAE and EAE. The exciter system comprises a remotely controllable function generator, a 3 kW broad band power amplifier, an impedance matching network, a power splitter and an isolation unit. The power distribution unit can drive 1, 2 or 4 saddle coils, allowing different combinations of antenna phasing which can preferentially excite specific, low toroidal mode numbers (n) and poloidal symmetry.

Maximum current and voltage applied to the saddle coils are of the order of 30 A and 500 V. The corresponding magnetic perturbations in the plasma core are calculated to be small, $\delta B/B_{tor} < 10^{-5}$ [17], and are expected neither to perturb the plasma significantly in the form of enhanced transport of energetic particles, nor to produce any non-linear wave or particle effects.

The diagnostic method requires repetitive sweeps of the driving frequency across a chosen range of interest in the region of the Alfvén continuum gap frequency. The plasma response is determined in terms of driven oscillating quantities such as magnetic fields and densities. The driven component is extracted from background noise in various diagnostic signals using a set of synchronous detectors which provide the in phase and quadrature components of the signals, i.e. their real and imaginary parts in a complex representation. Several probing channels are equipped with this coherent detection; the voltages induced on the unexcited saddle coils and the poloidal pick-up coils measure the perturbation of the radial and poloidal magnetic fields at several locations, allowing a mode analysis in the poloidal and toroidal conjugate plane. The time and frequency resolution of the frequency and damping measurements are interdependent and linked to the frequency sweep rate. The latter is limited on the upper side by the intrinsic plasma noise level and the integration time needed to extract the driven signal in the synchronous detection chain, and on the lower side by the characteristic time scale for variations of the plasma parameters which define the resonant frequency. Typical figures for the time and frequency resolutions in the plasmas studied are 100-500 ms and <1 kHz respectively, with sweep rates of the order of 200 kHz/s.

The synchronous detection chain can also be used in a passive mode, with the reference frequency still being swept, but with no current driven in the saddle coils, allowing unstable eigenmodes to be detected. When Neutral Beam Injection Heating at moderate power was applied, such passive measurements indicated broad band activity around the TAE frequency, defined as the centre of the gap: $f^0_{TAE} \cong v_{Alfvén}/(4\pi q R_0)$, where q is the safety factor and R_0 is the tokamak major radius.

In the following, we focus our attention on active measurements in the range 60-180 kHz performed in the ohmic phase of JET deuterium discharges. Several global eigenmodes have been clearly observed in different plasma conditions. An example of a resonance detected on one of the magnetic field probes is shown in Fig. 1. The signal amplitude, normalised to the complex amplitude of the current driven in the active antenna, describes a circle in the complex plane as the frequency is swept across the resonance. The maximum value of the oscillating magnetic field measured by the coil is of the order of 10^{-7} T for driving currents of the order of 5A in each antenna. This resonance behaviour was seen simultaneously on all of the magnetic field pick-up coils, as well as on the unexcited saddle coils.

The transfer function between the driving current and any particular diagnostic signal can be directly derived from the raw data by normalising that signal response to the antenna current. The presence of an Alfvén eigenmode manifests itself as a resonance in this transfer function, H, which can be represented in terms of complex conjugate poles, p_k and p_k^*, and residues, r_k and r_k^*

$$H(\omega, x) = \sum_{k=1}^{N} \frac{1}{2}\left(\frac{r_k(x)}{i\omega - p_k} + \frac{r_k^*(x)}{i\omega - p_k^*}\right) + D(\omega, x) = \frac{B(\omega, x)}{A(i\omega)}$$

Here N is the number of resonances in the measurement range, ω is the driving frequency and x is the measurement position. For the k^{th} resonance, $p_k = i\omega_{0k} + \gamma_k$ defines a pole which is common to all diagnostic signals, with ω_{0k} being the resonant (real) frequency and γ_k the damping rate. Since the signals may contain a direct, non-resonant coupling with the antenna, an additional scalar quantity D is added to the first order resonance terms.

The data from a complete set of diagnostic signals are analysed by simultaneously fitting the above expression to all of the signals, with a single denominator A which determines the resonance characteristics and separate numerators B [18]. By imposing a pole common to all transfer functions, the statistical errors in the evaluation of the poles are reduced and the estimates of the residues are then reliable even for noisy signals. The fitted pole provides two pieces of information. Its imaginary part gives the frequency of the mode, $f_{obs} = \omega_{0k}/2\pi$. Its real part, in the case of stable modes, is the algebraic difference between the damping rate and the growth rate: $\gamma = \gamma_{damping} - \gamma_{drive}$. In particular, if no fast particle driving terms are present in the plasma, $\gamma_{drive} = 0$ and γ corresponds directly to the damping rate of the mode, which is the case of the data shown in Fig. 1. For those diagnostic signals which are space-resolved measurements of the vacuum wave field, the residues correspond directly to the wave amplitude as a function of space, i.e. to the single mode structure.

The result of this fitting procedure applied to the experimental response shown in Fig. 1 is illustrated superimposed on the raw signals. With the numerator and denominator chosen to be of order 5 and 2, the fit provides an accurate value for the eigenmode frequency f_{obs} =144.2 +-0.1 kHz and for its damping rate $\gamma/2\pi$ = 1400 +-

100 s^{-1}. In this case the resonance quality factor was relatively large, $Q \sim \omega/\gamma \sim 125$, corresponding to relatively weak damping, $\gamma/\omega \sim 0.8\%$.

The 'Alfvén' character of the measured resonances was verified from the dependence of the observed resonance frequency on the magnetic field and density in many discharges, of which we describe two examples. Figure 2 shows the first, in which the toroidal magnetic field was varied from 2.2 to 3.0 T during the discharge, other parameters being held constant. The measured frequency agrees well with f^0_{TAE} evaluated assuming $q=1.5$, corresponding to the most effectively driven TAE mode [17,19], and using the line-averaged plasma density ($\bar{n}_e$) for calculating $v_{Alfvén}$. The damping coefficient varied as a function of the resonant frequency in such a way that γ/ω remained roughly constant at $\gamma/\omega \sim 1\%$. Figure 3 shows the second, in which the density was varied while maintaining both toroidal field and plasma current practically constant. The observed mode frequency again followed f^0_{TAE}. The damping of the mode decreased with increasing density and was much higher in this case, with $3\% < \gamma/\omega < 10\%$. A direct dependence of the eigenmode frequency on the plasma current was found over several discharges, indicating an inverse q dependence of the resonance frequency. These observations taken together clearly demonstrate that the observed driven resonances are Toroidicity induced Alfvén Eigenmodes.

The reconstruction of the TAE mode structure in the poloidal and toroidal directions is shown in Fig. 4, for a discharge with two upper saddle coils driven in phase situated 180^0 apart toroidally, providing mostly $|n|=2$ excitation. The phase of the residue of the response of the magnetic probes has a clear $|n|=2$ standing wave structure. The $n=+2$ and $n=-2$ components are excited with identical amplitudes, the toroidal symmetry being maintained both by the excitation and by the plasma itself in the

absence of significant toroidal rotation. The poloidal mode structure indicates a nodal point at the tokamak mid-plane, in agreement with numerical and analytical estimates for typical TAE spatial field structures [17,19].

Several possible damping mechanisms for TAE modes have been proposed. Firstly, continuum damping occurs when the eigenmode frequency intersects a shear Alfvén wave continuum at a resonant layer within the plasma. The damping by that continuum is independent of the details of the absorption mechanisms for the continuum itself but is very sensitive to the profiles q(r) and $\rho(r)$, where r is the minor radius of the magnetic surfaces on the tokamak mid-plane. Specifically, as the gaps are centred at the local value of f^0_{TAE}, continuum damping is linked to the radial dependence of the quantity $g(r)=1/(q(r)\rho(r)^{1/2})$. If g(r) is approximately constant, the gaps are aligned and the continuum damping should be minimised. If g(r) varies strongly with r, continuum damping should become dominant and lead to large damping rates, $\gamma/\omega \sim 5\text{-}10\%$ [20,21]. Secondly, in the absence of strong continuum damping, several kinetic effects may become important. Landau damping effects are mainly due to the mode interaction with bulk ions and electrons, when $v_{th||} \sim v_{Alfvén}$ or $v_{th||} \sim v_{Alfvén}/3$. Ion Landau damping scales as $\gamma_i/\omega \propto \beta_i^{-3/2} \exp(-1/(9\beta_i))$ [22], $\beta_j = n_j T_j/(B_{tor}^2/(2\mu_0))$ being the ratio between the pressure of the species j (j=i, e) and the magnetic field pressure. γ_i is negligibly small for the ohmic discharges considered, whereas for these relatively cold and dense plasmas, $v_{the||} \sim v_{Alfvén}$ and thus electron Landau effects can contribute significantly to the damping, $\gamma_e/\omega \propto \beta_e v_{Alfvén}/v_{the||}$ [5]. Damping can also be produced by trapped electron collisional absorption, occurring during the transition from trapped to passing orbits, caused by collisional pitch-angle scattering, and yielding $\gamma_e^t/\omega \propto (\nu_e/\omega)^{1/2} (\beta_e q^2 + 0.1(\rho_s/\Delta_{TAE})^2)$ [23,24]. Here $\nu_e \sim n_e/T_e^{3/2}$ is the electron collision frequency,

$\rho_s^2=2T_e/m_i\omega_{ci}^2$ and $\Delta_{TAE}^2=\pi^2/64\ (r\varepsilon/m)^2$, with ω_{ci} being the ion cyclotron angular frequency, ε the tokamak inverse aspect ratio and m the poloidal mode number. Finally, a contribution to the Alfvén eigenmode absorption can come from radiative damping [25], which is a finite Larmor orbit effect of the bulk ions and leads to $\gamma_R/\omega \propto s^2 \exp(-f(s,\varepsilon)/\rho_i m)$, where f is a function of the magnetic shear s ($s=r/q\ dq/dr$) and the inverse aspect ratio, and ρ_i is the ion Larmor radius.

Greatly differing damping rates were measured in two similar discharges with different g(r). Figure 5 shows the radial dependence of g(r) obtained from the reconstructed equilibrium and the density profiles, together with the two measured eigenmodes and their damping rates. When there was a strong radial dependence of g(r), Fig. 5 curve (a), the gaps were not aligned through the continuum structure and strong damping occurred with $\gamma/\omega \sim 5\%$, in agreement with prior theoretical estimates of continuum damping [21]. The discharge already shown in Fig. 3 also exhibited a strong variation of g(r) and strong damping. The g(r) profile in Fig. 5 curve (b) was flatter and led to a more 'open' gap structure and therefore to a much less effective continuum damping. The absorption mechanism in this case, has to be sought in the kinetic interactions.

Damping rates were measured in a wide variety of conditions, with $1\ MA<I_p<3$ MA, $1x10^{19}\ m^{-3}<\bar{n}_e<5x10^{19}\ m^{-3}$ and $1\ T<B_{tor}<3.5$ T. The results with both odd and even low-n excitation span several orders of magnitude, from $\gamma/\omega<0.1\%$ to $\gamma/\omega>10\%$, suggesting that different absorption mechanisms dominate according to the configuration of each specific shot. This extreme sensitivity of the damping rates of the TAE to the details of the plasma equilibrium profiles make comparisons with theoretical predictions very difficult. Even in the case of flat g(r) profiles, the measured damping

appears to be at least a factor of two larger than that calculated by local models considering electron Landau and electron collisional damping in the particular case of low mode numbers. Contributions from either continuum damping at the plasma edge or by radiative damping in the core must therefore be significant and have to be accounted for.

The combination of external excitation using the JET saddle coils as antennas and synchronous detection of the diagnostic response forms the basis of the new active diagnostic for Alfvén eigenmodes on JET. The successful implementation of this diagnostic method has allowed us to drive Toroidicity induced Alfvén Eigenmodes in linearly stable conditions and to identify them by their frequency dependence on the density and the toroidal magnetic field. Control of the antenna phasing together with space resolved magnetic wave field measurements has allowed both the selection and the identification of the driven mode structure. The damping rates of the Toroidicity induced Alfvén Eigenmodes have been experimentally measured for the first time. The large range of the measured values of γ/ω indicates the capability of the diagnostic method, highlights the effectiveness of different MHD and kinetic Alfvén eigenmode absorption mechanisms, and provides a useful test for the theories being developed and refined to assess the stability of Alfvén eigenmodes in future ignition experiments.

The Authors thank the members of the JET Team for experimental support. This work was partly supported by the Fonds National Suisse pour la Recherche Scientifique, within the JET/CRPP-EPFL Task Agreement 394.

References

[1] C.Z. Cheng, L.Chen and M.S.Chanse, *Ann. Phys.* (New York) **161**, 21 (1985).

[2] R.Betti, J.P.Freidberg, *Phys. Fluids B* **3**, 1865 (1991).

[3] M.S.Chu et al., *Phys. Fluids B* **4**, 3713 (1992).

[4] A.D.Turnbull et al., *Phys. Fluids B* **5**, 2546 (1993).

[5] G.Y.Fu and J.W.Van Dam, *Phys. Fluids B* **1**, 2404 (1989).

[6] H.H.Duong et al., *Nucl. Fusion* **33**, 749 (1993).

[7] K.L.Wong et al., *Phys. Rev. Lett.* **66**, 1874 (1991).

[8] W.W.Heidbrink et al., *Nucl. Fusion* **31**, 1635 (1991).

[9] S.Ali-Arshad and D.J.Campbell, to be published on *Plasma Phys. and Controlled Fusion.*

[10] W.W.Heidbrink et al., *Phys. Rev. Lett.* **71**, 855 (1993).

[11] E.Fredrickson et al., *Proc. of XV Int. Conf. on Plasma Phys. and Contr. Fusion, IAEA*, Seville, Spain (1994).

[12] A.Fasoli et al., *ibidem.*

[13] G.A.Collins et al., *Phys. Fluids B* **29**, 2260 (1986).

[14] G.A.Collins et al., *Plasma Phys. Contr. Fusion* **29**, 324 (1987).

[15] P.Descamps et al., *Phys. Lett.* A **143**, 313 (1990).

[16] A.Tanga et al., *Plasma Phys. Contr. Fusion* **36**, B39 (1994).

[17] G.Huysmans et al., *Proc. XX Eur. Conf. on Controlled Fusion and Plasma Physics,* ed. by J.A.Costa Cabral, M.E.Manso, F.M.Serra, F.C.Schuller, EPS Lisbon, (1993) **I**, 187.

[18] J.-M.Moret, *CRPP Laboratory Report* LRP 498/94 (1994).

[19] L.Villard et al., *Proc. XX Eur. Conf. on Controlled Fusion and Plasma Physics,* ed. by J.A.Costa Cabral, M.E.Manso, F.M.Serra, F.C.Schuller, EPS Lisbon, (1993) **IV**, 1347.

[20] L.Villard and G.Fu, *Nucl. Fusion* **32**, 1695 (1992).

[21] S.Poedts et al., *Plasma Phys. Contr. Fusion* **34**, 1397 (1992).

[22] R.Betti, J.P.Freidberg, *Phys. Fluids B* **4**, 1465 (1992).

[23] N.N.Gorelenkov and S.Sharapov, *Physica Scipta* **45**, 163 (1992).

[24] J.Candy and M.N.Rosenbluth, *Plasma Phys. Contr. Fusion* **35**, 957 (1993).

[25] R.R.Mett and S.M.Mahajan, *Phys. Fluids B* **4**, 2885 (1992).

Figure captions

Fig. 1 Example of a TAE resonance in the ohmic phase of JET shot #31638. Left: Real and imaginary parts of a magnetic probe signal response. Right: Complex plane representation of the same signal. In both cases the signals are normalised to the driving current. The fit with B and A of order 5 and 2 is also shown, giving f=144.2 +-0.1 kHz, $\gamma/2\pi$=1400 +-100 s^{-1}. $B_{tor} \cong 2.8$ T, $I_p \cong 2.2$ MA, $\bar{n}_e \cong 3x10^{19}$ m^{-3}; two upper saddle coils were used, in phase and 180^0 apart toroidally.

Fig. 2 Variation of the measured eigenmode frequency with toroidal magnetic field in JET shot #31591. B_{tor} varied linearly with time between 2.2 and 3 T while the density and plasma current were kept constant; the same saddle coils were used as in Fig. 1, but with opposite phase; f^0_{TAE} is calculated for q=1.5.

Fig. 3 TAE frequency (a) and γ/ω (b) for different densities within JET shot #31150. $\bar{n}_e$ varied between $5.2x10^{19}$ m^{-2} and $11x10^{19}$ m^{-2}; $B_{tor} \cong 2.7$ T, $I_p \cong 2$ MA; one upper saddle coil was driven.

Fig. 4 Toroidal and poloidal mode structure of a TAE, represented as the magnitude (+) and phase (x) of the residues fitted to the poloidal field pick-up coil signals. The magnetic signals are normalised to the active saddle coil current. The driven spectrum, $|n|=2$, and the plasma parameters were the same as in Fig. 1. The poloidal angle is measured from the tokamak outer mid-plane upwards. The toroidal extension of the JET saddle coils is indicated as a shaded region.

Fig. 5 The relationship between the profile of $g(r)=1/(q(r)\rho(r)^{1/2})$ and the damping of TAE modes. g(r) and the raw and fitted frequency responses of a normalised magnetic probe signal are shown for two discharges. Strong damping occurs when g(r) has a strong radial dependence (a), and weak damping when g(r) is flat (b). Excitation peaked at $|n|=2$ was used for both discharges; measurements were taken at the same time in the ohmic phase with similar plasma configuration; $\bar{n}_e \cong 4\text{x}10^{19}$ m^{-3} ; (a) $B_{tor} \cong 1.8$ T, $I_p \cong 2$ MA. (b) $B_{tor} \cong 2.8$ T, $I_p \cong 2.3$ MA.

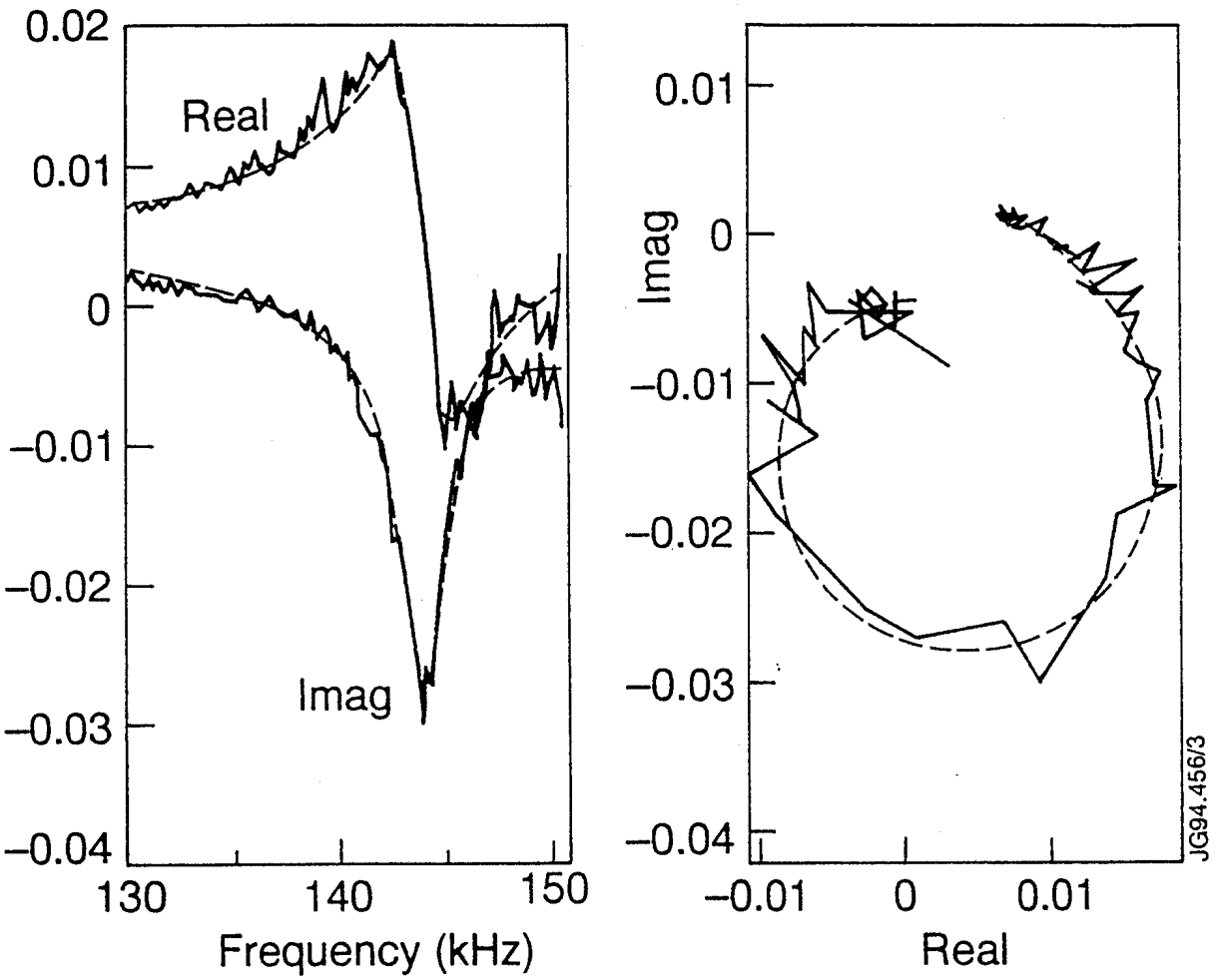
0.02
0.01
0
−0.01
−0.02
−0.03
−0.04
Real
Imag
130
140
150
Frequency (kHz)
0.01
0
−0.01
−0.02
−0.03
−0.04
Imag
−0.01
0
0.01
Real
JG94.456/3

Fig. 1

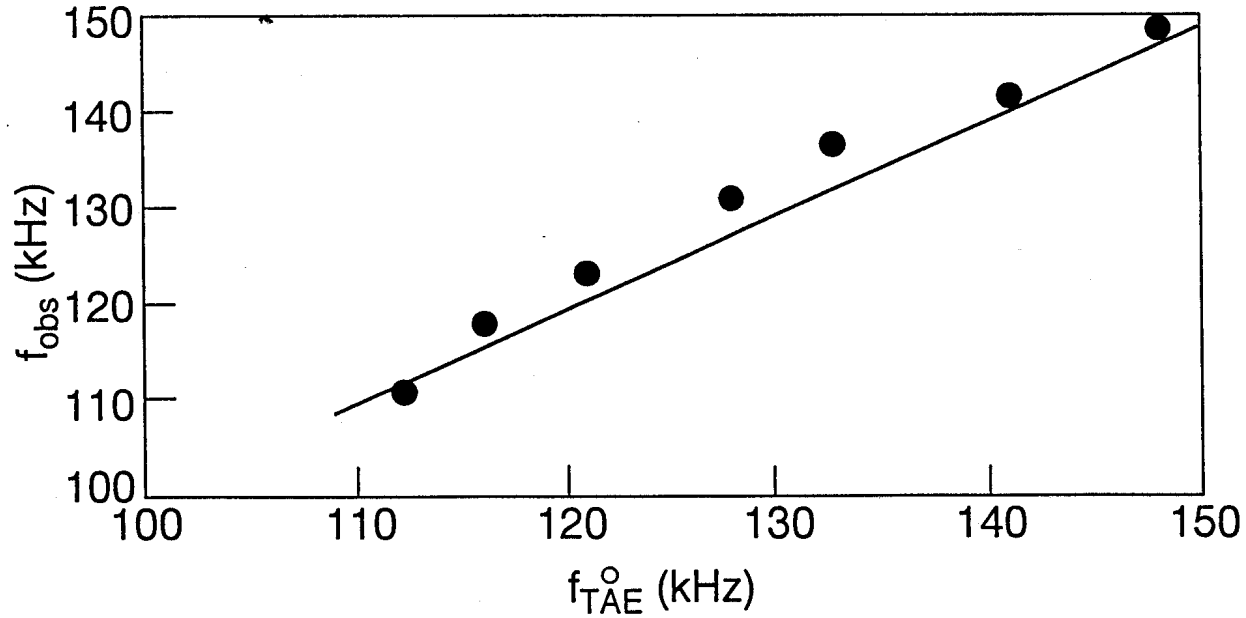
150
140
130
120
110
100
f_{obs} (kHz)
100
110
120
130
140
150
f°_{TAE} (kHz)

Fig. 2

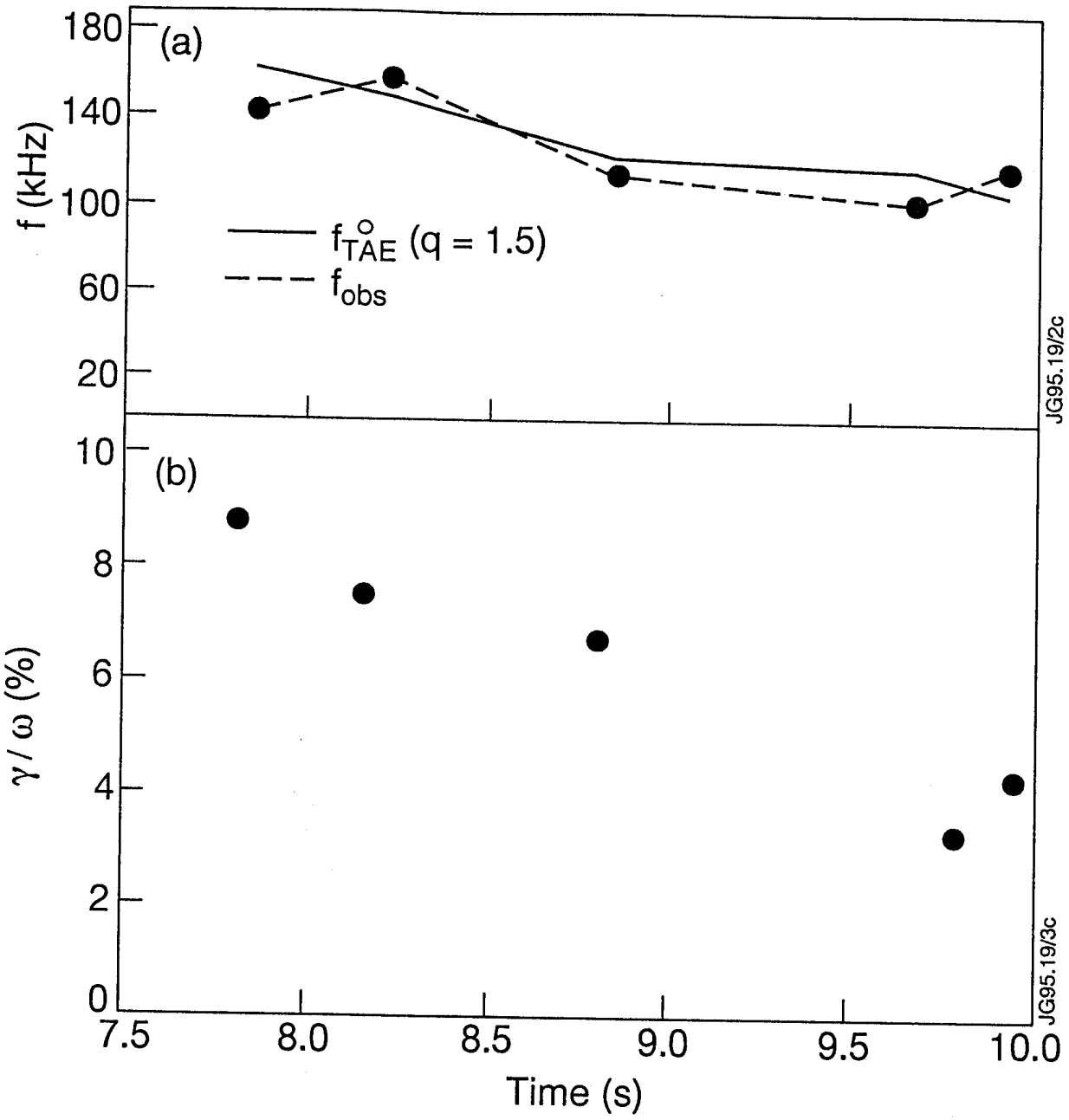
(a)
f (kHz)
180
140
100
60
20
f°_{TAE} (q = 1.5)
f_{obs}
JG95.19/2c
(b)
γ / ω (%)
10
8
6
4
2
0
7.5
8.0
8.5
9.0
9.5
10.0
Time (s)
JG95.19/3c

Fig. 3

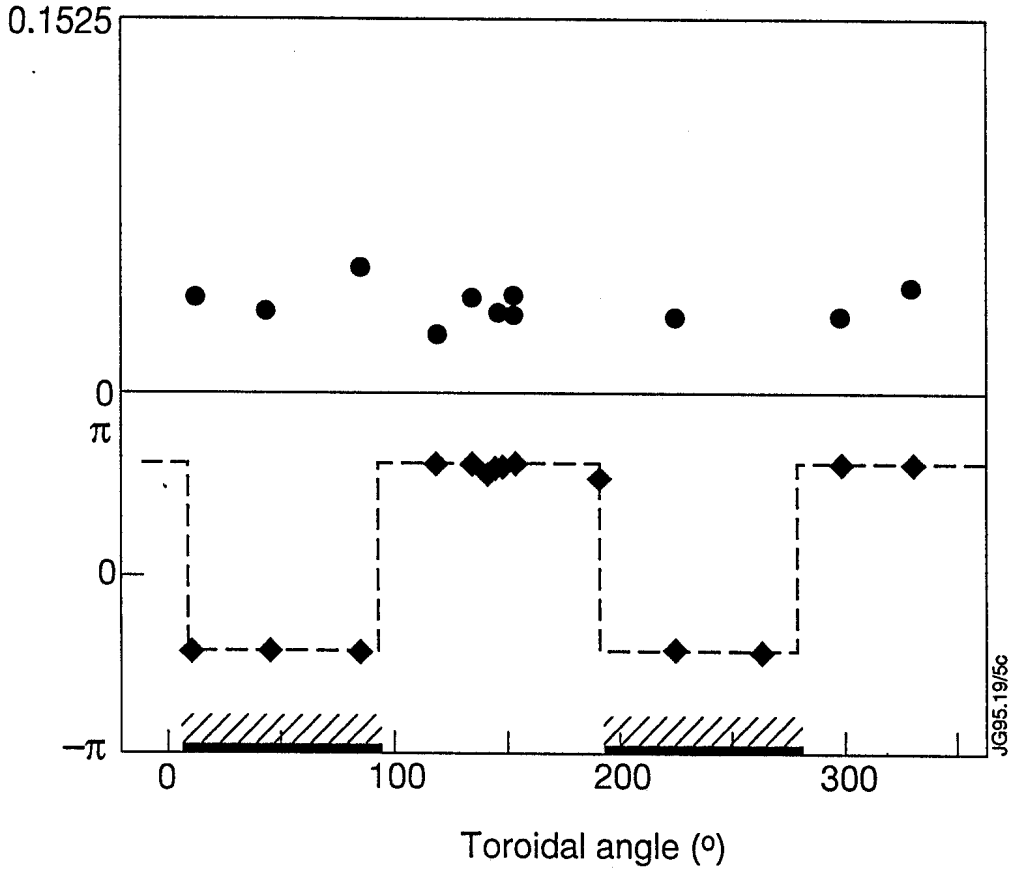
0.1525
0
π
0
−π
0
100
200
300
Toroidal angle (°)
JG95.19/5c

Fig. 4

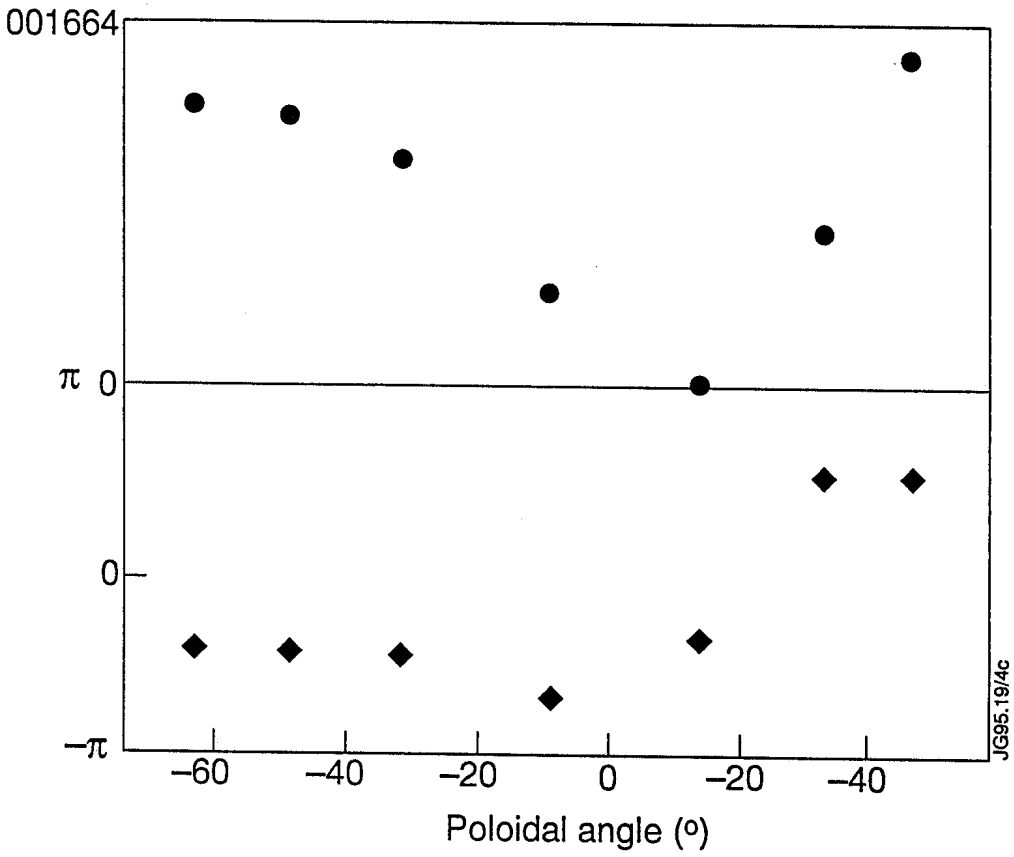
001664
π 0
0
−π
−60
−40
−20
0
−20
−40
Poloidal angle (°)
JG95.19/4c

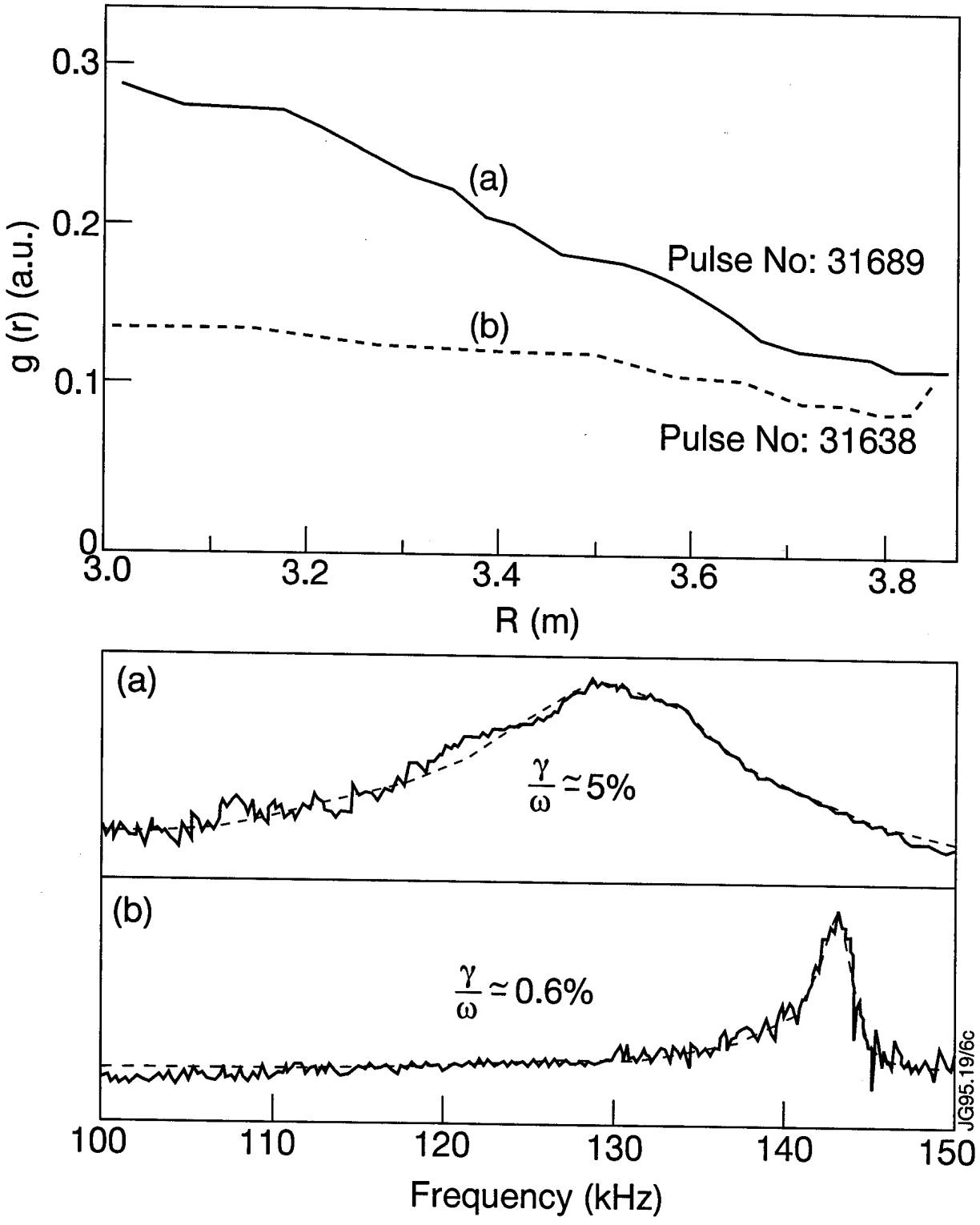
0.3
0.2
0.1
0
g (r) (a.u.)
(a)
Pulse No: 31689
(b)
Pulse No: 31638
3.0
3.2
3.4
3.6
3.8
R (m)
(a)
γ/ω ≃ 5%
(b)
γ/ω ≃ 0.6%
JG95.19/6c
100
110
120
130
140
150
Frequency (kHz)

Fig. 5